Loss current minimization during ion extraction from an inductively coupled plasma

Oleksiy Vozniy,[a),b)] Kostyantyn Polozhiy,[b)] and Geun Young Yeom
Department of Nanotechnology, Sungkyunkwan University, Jangan-Gu Chunchun-Dong 300, Suwon 440-746, South Korea

(Received 5 July 2007; accepted 30 August 2007; published online 26 October 2007)

In ion sources with a grid-type acceleration system, the output current often decreases with increasing power at a constant extraction voltage despite the fact that the carrier density inside the source increases linearly. At this point, the loss and output currents have the same magnitude. This paper proposes a mechanism for loss current minimization when restrictions are placed on the beam focusing efficiency with increasing rf power. The influence of the plasma potential on the magnitude of the loss current was examined. The beam intensity was found to increase considerably when the plasma potential was sufficiently high to suppress sheath curvature growth. © *2007 American Institute of Physics*. [DOI: 10.1063/1.2800842]

I. INTRODUCTION

Inductively coupled plasma (ICP) is a commonly used instrument for film deposition and etching.[1–4] Because of its ability to produce high-density plasma at low pressure, it has a number of apparent benefits compared with discharges using an electrode principle of low temperature plasma generation. The discharge is ignited and maintained by the electrical heat of ring induction currents flowing in ionized gas along the force lines of the eddy field.[5] Ultrapure plasma, which is not exposed to the products of the electrode erosion, can be created thereby allowing one to work with chemically active gases for an unlimited period of time. The plasma parameters, such as pressure, integral current, and frequency, can be changed over a wide range providing optimal conditions for plasma processing.

Taylor *et al.*[6] proposed a grid method of ion acceleration, where the plasma is limited by the field of the positive electrode, which that increases the plasma potential up to the required level. Due to the grid transparency and the fact that the plasma potential is higher that the electrode voltage, ions escape from the source and form an almost parallel beam. The angular distribution of the beam depends on the sheath structure near the grid and can be controlled by the second negative electrode potential.

In the absence of ion losses, the continuity law between the Bohm current near the sheath and the current determined by the Child-Langmuir equation limits the maximum beam current. Although the energy of the beam is preset by the first electrode voltage V_1, it is always higher than the magnitude eV_1 due to the plasma potential, which can significantly shift the ion energy distribution function (IEDF) to higher energies.[7,8] The difference between the plasma V_p and the first electrode V_1 potentials defines the additional ion energy, which can reach several tens of eV at a pressure ranging from 10^{-2} to 10^{-3} Torr and an accelerating voltage of 400 V. Larger beam energy deviations from the preset values are observed at higher accelerating voltages and lower pressures.[9]

At pressures $>10^{-2}$ Torr, IEDF perturbation can also be observed due to the increasing role of inelastic collisions of ions with the atoms of residual gas. At that distribution, the function becomes broader acquiring additional maxima.[10] Multiple peaks of IEDF are also observed when the amplitude of the ion oscillations in a rf field is comparable to the sheath length.[11]

An inverse effect is often observed at its output at high extraction voltages, even when the ion density inside the source increases, for example, because of pressure or rf power growth. This is because the ions from ion beam defocusing suffer collisions with the second and third grids, which leads to a decrease in current density.

It is possible to minimize the loss current at a given pressure and accelerating voltage due to electrostatic focusing.[12,13] However, the source output current is limited at higher rf power due to the complications of controlling the heath geometry and ion trajectory.

This study examined the influence of the plasma potential on the loss current, the magnitude of additional ion energy, and the IED.

II. EXPERIMENTAL SETUP

Figure 1 shows the experimental setup. An rf discharge in an external ICP ion source was induced by 13.56 MHz

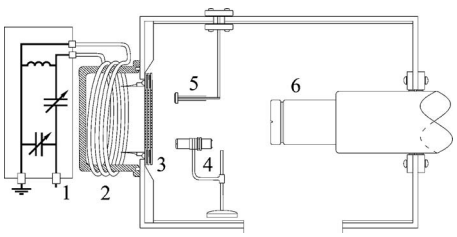

FIG. 1. Experimental Setup. (1) rf input, (2) three-turn induction coil, (3) extraction grids, (4) Faraday cup, (5) planar Langmuir probe, and (6) QMS inlet.

[a)]Electronic mail: oleksiy@skku.edu
[b)]Also at Kharkiv Scientific Center of Physics and Technologies, Ukraine.

oscillations of an electromagnetic field. The rf voltage from the generator to a three-turn antenna was applied through a standard π-type matching network. For better plasma stability, additional inductance was shunted with the antenna. The diameter of the discharge volume was 100 mm with a length of 65 mm.

Ion extraction from the plasma was carried out using three graphite grid electrodes. The thickness of the electrodes and distance between them were 1 and 3.0 mm, respectively. The 2 mm holes were drilled in a hexagonal raster. Since the geometrical transparency of the grid electrodes was 60%, they also served as a barrier for gas atoms. This allows a sufficiently high pressure to be maintained inside the source for plasma generation, whereas ions suffered almost no collisions at the beam transportation region.[14] The maximum integral current of the ICP ion gun reached 120 mA at the source outlet.

The set of diagnostic tools included a quadrupole mass spectrometer (Hiden Analytical) with an integrated energy analyzer allowing measurements of the ion energy from 0 to 1000 eV with a resolution 0.05 eV, a Faraday cup, and a single planar Langmuir probe that was connected to the scheme of rf noise reduction.

III. RESULTS AND DISCUSSION

The ion trajectory in an electric field of grid electrodes for the two-dimensional case is given by a set of equations,

$$\frac{d^2x}{dt^2} = \frac{q_i}{m_i}E_x(x,y),$$
$$\frac{d^2y}{dt^2} = \frac{q_i}{m_i}E_y(x,y). \tag{1}$$

Here, q_i and m_i represent the ion charge and mass, respectively. $E_x(x,y)$ and $E_y(x,y)$ are the components of an electric field.

The nonparametric equation of the ion trajectory was obtained by reducing the number of variables by illuminating the time t and introducing $y'=dy/dx$ and $y''=d^2y/dx^2$ as follows:

$$\frac{2\Delta U}{1+(y')^2}y'' + E_x y' - E_y = 0. \tag{2}$$

Here, ΔU is the potential energy change in the ion. If the origin is chosen at the distance of the sheath layer h from the first grid, $\Delta U = V_p - V(x) + \varepsilon$, where ε is the ion initial energy and V_p the plasma potential.

Equation (2) can be reduced to

$$2\zeta y'' + \zeta' y' + \zeta'' y = 0, \tag{3}$$

where ζ is the first coefficient of serial expansion in y for the potential energy in the neighborhood of the x axes. ζ and ζ'' are the first and second derivatives of this magnitude with respect to x. Equation (3) is valid only in the neighborhood of the x axis and generally has a solution only for several simple forms of the function ζ.[15] Numerical integration of the differential equation in the simplest case (where the field from both sides of the electrode is uniform and the particle begins to move in the shadowed region of Fig. 2) shows that the equation describes the motion trajectory within a few percent of the trajectory given by Eq. (3).

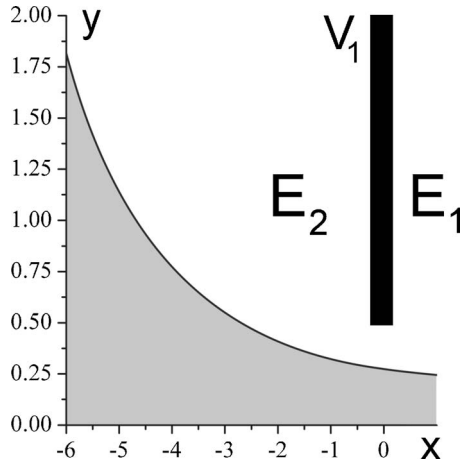

FIG. 2. Paraxial region, where the linearization of Eq. (3) of the ion trajectory is possible.

The problem of finding the ion trajectory under the influence of the second electrode can be simplified using the Schwarz-Christoffel transformation. The mapping function, which defines the transition from $z=x+iy$ plane to $w=u+iv$ plane, is given by

$$z = -ip\left(W + \frac{1-a^2}{2a}\ln\frac{W+a}{W-a}\right), \tag{4}$$

where the constants p and a are related by the following set of equations:

$$p = \frac{2ad}{\pi(1-a^2)},$$
$$1 - \frac{1}{2p} = \frac{1-a^2}{2a}\ln\frac{1-a}{1+a}, \tag{5}$$

where d is measured in units of the hole diameter h. Therefore, the potential distribution in the w plane, defining the ion trajectory, is given by

$$V = pE_1 v + \frac{\Delta U}{\pi}\left(ctg\frac{v}{u-a} - ctg\frac{v}{u+a}\right). \tag{6}$$

Figure 3 shows several typical ion trajectories, which were obtained by a reciprocal transformation, where the full curves represent the case when $d=h$, and the broken curves represent the case when $d=3h$.

In order to determine the values of the loss current, it is necessary to consider the continuity law of the current at the transition region between the bulk plasma and the space where the ions are accelerated in an electrical field of the grid electrodes (Fig. 4). The ion current in the plasma is limited by the Bohm criterion,

$$j_b \cong 0.6en_e\left(\frac{kT_e}{m_i}\right)^{1/2}, \tag{7}$$

Outside the plasma, the ion current is determined by the Child-Langmuir law,

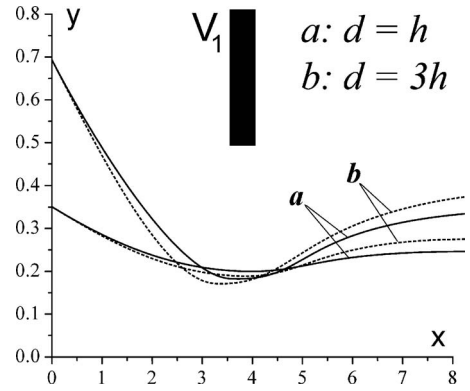

FIG. 3. Typical ion trajectories under the influence of the second grid at different distances from the first grid. The field is kept constant.

$$j_i = \frac{1}{9\pi l^2}\left(\frac{2e}{m_i}\right)^{1/2} U^{3/2}, \tag{8}$$

which is a solution of Poisson's equation $\nabla^2 U = -\rho/\varepsilon_0$ at low pressures.[16] Here, l is the sheath length, and U is the plasma potential relatively to the electrode potential, which is averaged over the period of rf oscillations.

Plasma surface indentation takes place during the increase in focusing potential between the first and the second electrodes because the condition $j_b = j_i$ should be fulfilled. When j_b becomes smaller than j_i, local radius of the plasma surface (meniscus) near the grid holes decreases. Ideal focusing occurs when the angle, which a tangent to the surface touches the x axis, γ_{pv}, is sufficiently high. Overfocusing occurs during further increases in the potential difference between the first and the second electrode leading to an increase in ion loss on the grids. Whether the ions will collide with the second electrode passing through the first grid at the optimal extraction voltage depends on the distance r_0 from the x axis that the ions enter the sheath layer and on the angle γ_{pv}.

At pressures $>10^{-2}$ Torr, ion movement in the sheath is not strictly collisionless. It is more appropriate to use the following equation for the ion current j_i in the continuity law instead of Eq. (8):[17]

$$U = \frac{6h^{4/3}}{5} \cdot \left(\frac{m_i}{2e} \cdot \frac{h+\lambda_i}{\lambda_i}\right)^{1/3} \cdot \left(\frac{h+\lambda_i}{2h+\lambda_i}\right) \cdot (6\pi j_i)^{2/3}, \tag{9}$$

where λ_i is the ion mean free path, and $U = V_p - V_1$.

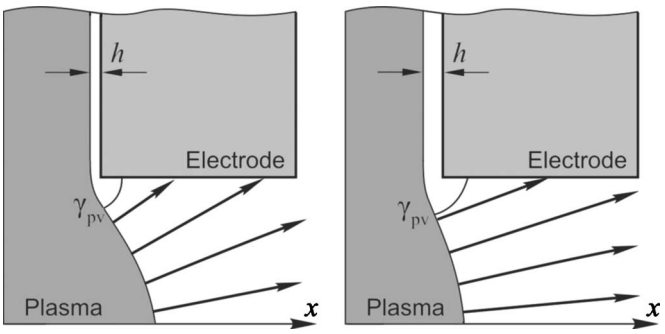

FIG. 4. Schematic geometry of the plasma surface position near the first electrode.

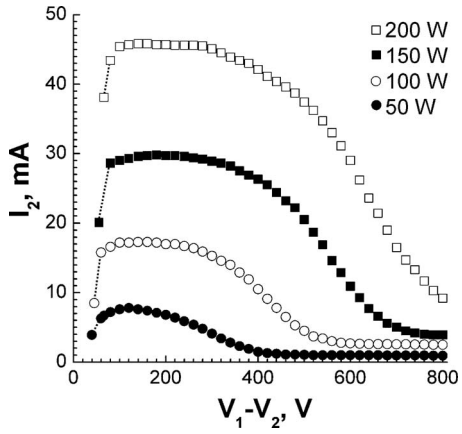

FIG. 5. Loss current collected from the second electrode as a function of focusing potential. Hole size is 2 mm.

In order to minimize the loss current on the second electrode, it is sufficient to determine the optimal focusing potential $V_1 - V_2$, which can be maintained at any acceleration voltage V_1, since the magnitude of the loss current I_2 weakly depends on it.

Figure 5 shows the loss current dependence on the voltage difference between the first and the second grids. The electrode was biased with a small negative potential to cut off the possible electron current.

As shown in Fig. 5, when the rf power increases, the minimum of the loss current shifts to higher voltages, which limits the source output current. Beginning from $\Delta V = V_1 - V_2 = 80$ V, the constant value of the loss current was observed following by its monotone decrease. The magnitude of the decrease becomes lower at higher power. Therefore, for the power of 50 W, it is necessary to apply 400 V for sufficient focusing but more than 900 V is required for 200 W.

The electrode hole size also places limitations on the low value of the loss current. When it becomes smaller, the current can be decreased by the plasma surface position only within 10%–20%. Figure 6 shows the loss current dependence of the grids with holes 1 mm in diameter. The distance between the holes was increased to 4 mm, and the rf power was varied from 60 to 200 W.

As shown from the image, ion source focusing became

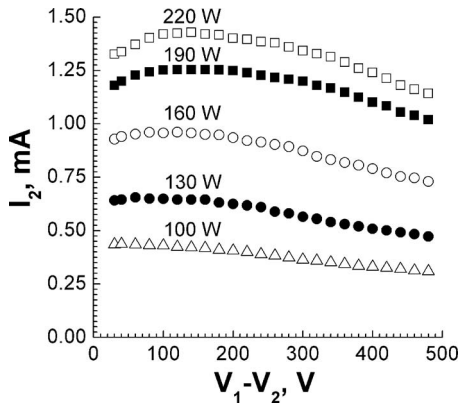

FIG. 6. Loss current collected from the second electrode as a function of the focusing potential. Hole size is 1 mm.

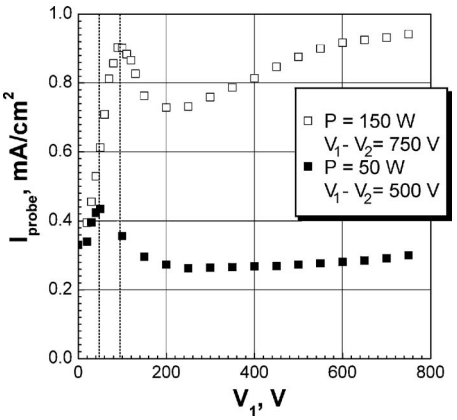

FIG. 7. Output ion current measured using a Faraday cup as a function of the first grid voltage for 150 W (upper curve) and for 50 W (bottom curve) with V_1-V_2 equal 750 and 500 V, correspondingly.

less effective in the whole range of applied accelerating voltages. Therefore, at 220 W, only 20% of ions from the total loss current escaped collision with the second electrode due to electrostatic focusing. This magnitude reached 80% in the case of a large hole diameter.

The second grid current cannot provide comprehensive information on the total ion loss because some of the ions are lost on the third grounded electrode. A planar Langmuir probe was used to control the source output ion flux at a distance of 5 mm from it. Figure 7 shows the dependence of the collected current on the first grid voltage, while the focusing potential was maintained constant. The bottom graph shows the plot at a rf power $P=50$ W and $V_1-V_2=500$ V, and the upper graph shows a plot for $P=150$ W and $V_1-V_2=750$ V, i.e., at the optimal extraction voltages for the given power.

The output current dependences have peaks in the low energy region where the current loss on the third grounded electrode is at a minimum. The acceleration voltages, at which the source exhibits its optimal performance, are 40 and 90 V for an rf power of 50 and 150 W, respectively. The difference in the source output current peak position is believed to be the result of the plasma potential growth when the power increases. Ion current growth at acceleration voltages $V_1 \geqslant 200$ eV can be explained by secondary electron emission from the metal surface of the planar probe. Thus, the ion current growth at high energies is not connected to the source properties.

Figure 8 shows the evolution of the IED profiles as the focusing potential V_1-V_2 increases from 200 to 500 V. V_1 was maintained to be equal to +200 V, whereas V_2 was varied from 0 to −300 V. The upper profile represents the case of high beam defocusing. The ion losses on the second electrode decrease with increasing current j_i, which is determined by Child's law. In parallel with this process, the third grid current decreases by donating to the source integral current unless the maximum source output current is achieved. An ion energy peak was observed even at small focusing voltages but the ion energy spread in this case is high. The extraction voltage growth causes a significant increase in the

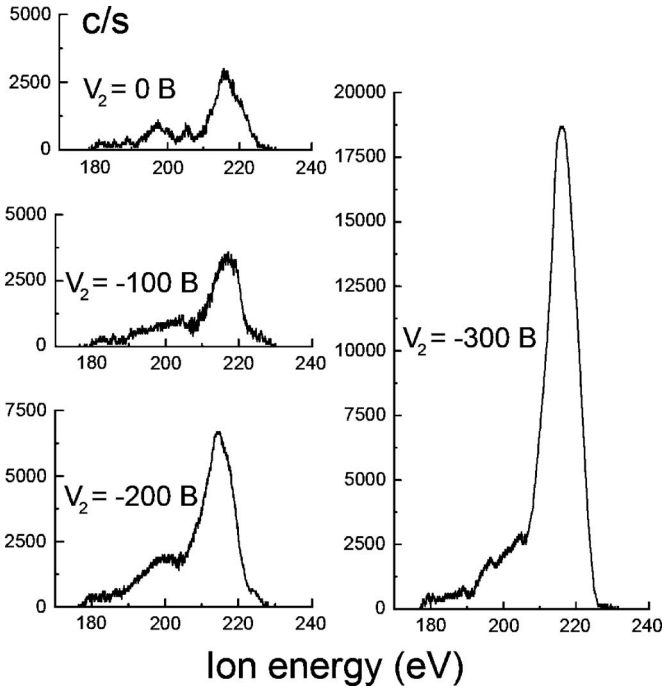

FIG. 8. Ion energy profile evolution with a potential difference increase between the first and the second electrodes.

beam intensity while the mean ion energy becomes close to the energy corresponding to the maximum of the IEDF.

It is important to define the loss current as a function of the plasma potential. Analyzing the IED, it is possible to estimate V_p with an accuracy of 3–5 eV. The beam energy is shifted by the magnitude of the plasma potential compared with the preset value of acceleration voltage. As shown in Fig. 8, the difference between the ion mean energy and the magnitude eV_1 equals 17 eV. This magnitude can reach 50 eV at the region of higher acceleration voltages and pressures, as shown in Fig. 9.

Figure 10 demonstrates an ion energy shift at a pressure ranging from 4×10^{-3} to 1×10^{-2} Torr at extraction voltages $V_1=410$ V and $V_2=200$ V, and $P=200$ W. During the pres-

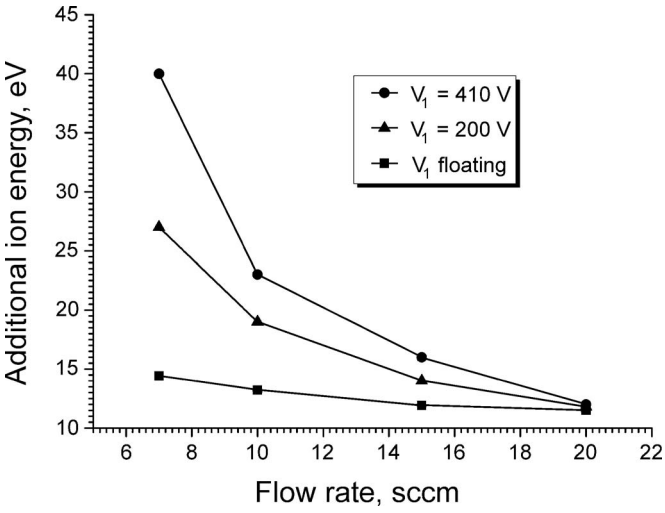

FIG. 9. Additional ion energy due to the plasma potential as a function of the argon flow rate.

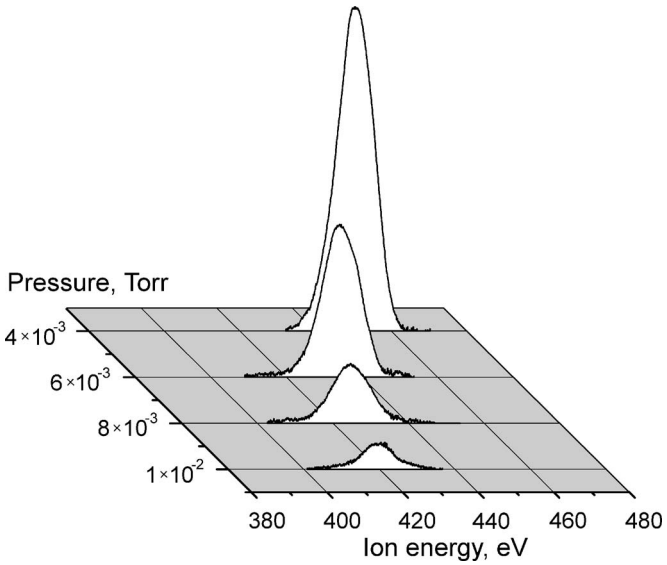

FIG. 10. Effect of beam energy shift caused by an increase in plasma potential as a function of pressure at acceleration voltage of 410 V.

sure increase, the higher rate of inelastic collisions of electrons with atoms leads to a decrease in electron temperature decrease. Therefore, fewer electrons escape to the walls and the plasma potential decreases. This is also accompanied by a decrease in beam intensity because a smaller plasma potential corresponds to a higher loss current.

IV. CONCLUSION

An ICP source output current limitation was observed as the power was increased at constant focusing potential. As the power increases, a higher focusing potential is needed to compensate for plasma surface movement. The plasma boundary position, which determines the loss current, was found to be affected by the rf power, pressure, and focusing voltage. At the same time, it showed a weak dependence on the acceleration voltage when the other parameters were constant.

It was found that a large loss current, which is caused by an increase in the angle of the plasma surface curvature, does not decrease the ion mean energy but leads to a broadening of the IED function. The ion beam intensity can be increased significantly by keeping the magnitude of the plasma potential within the range of 10–12 V compared with the first electrode voltage.

ACKNOWLEDGMENT

This study was supported by National Program for Tera-level Nanodevices of the Korea Ministry of Science and Technology as one of the 21st Century Frontier Programs.

[1] M. J. Kim, J. S. Lee, S. K. Kim, G. Y. Yeom, J. B. Yoo, and C. Y. Park, Thin Solid Films **475**, 41 (2005).
[2] A. M. Efremov, D. P. Kim, K. T. Kim, and C. I. Kim, Microelectron. Eng. **71**, 54 (2004).
[3] K. Suzuki and K. Kijima, Vacuum **80**, 519 (2006).
[4] W. Kulisch, P. Colpo, P. N. Gibson, G. Ceccone, D. V. Shtansky, E. A. Levashov, and F. Rossi, Surf. Coat. Technol. **188–189**, 735 (2004).
[5] O. A. Popov, *High Density Plasma Sources* (William Andrew Publishing/Noyes, Park Ridge, NJ, 1995), p. 77.
[6] R. J. Taylor, K. R. MacKenzie, and H. Ikezi, Rev. Sci. Instrum. **43**, 1675 (1972).
[7] K. H. Bai, C. K. Choi, and H. Y. Chang, Plasma Sources Sci. Technol. **13**, 662 (2004).
[8] K. H. Bai, J. I. Hong, S. J. You, and H. Y. Chang, Phys. Plasmas **8**, 4246 (2001).
[9] K. Okada, S. Komatsu, and S. Matsumoto, J. Vac. Sci. Technol. A **21**, 1988 (2003).
[10] B. Chapman, *Glow Discharge Processes* (Wiley, New York, 1980), p. 152.
[11] A. Ranjan, V. M. Donnelly, and D. J. Economou, J. Vac. Sci. Technol. A **24**, 1839 (2006).
[12] J. H. Whealton, R. W. McGaffey, and W. L. Stirling, J. Appl. Phys. **52**, 6 (1981).
[13] W. S. Cooper, K. Halbach, and S. B. Magyary, Computer-Aided Extractor Design Tech. Report No. LBL-3399, 1974 (unpublished).
[14] N. Umeda, T. Yamamoto, M. Hanada, L. Grisham, M. Kawai, T. Ohga, N. Akino, T. Inoue, M. Kazawa, and K. Kikuchi, Fusion Eng. Des. **74**, 385 (2005).
[15] N. Shibata, J. Phys. Soc. Jpn. **15**, 200 (1960).
[16] C. D. Child, Phys. Rev. **32**, 492 (1911).
[17] O. V. Vozniy, B. J. Park, K. S. Min, and G. Y. Yeom, J. Korean Phys. Soc. **50**, 1271 (2007).